Experimental nonmechanical image rotation to 20 angles using an acousto-optic dove prism

Yong-Seok 1m
Eung GI Paek
Xiao Tang
National Institute of Standards and Technology
Information Technology Laboratory
Gaithersburg, Maryland 20899-8951
E-mail: xiao.tang@nist.gov

Joon Y. Choe
Naval Research Laboratory
Radar Division
Washington, DC 20375

Tae K. Oh
Naval Surface Warfare Center
Dahlgren, Virginia 22448-5100

Abstract. An experimental demonstration of nonmechanical optical image rotation to 20 different angles is described. The optical system consists of a polygon mirror with 20 facets in a ha" cylinder and a 2-D acousto-optic beam deflector. Experimental details including the requirements of components are described. Various issues such as number of rotation angles, resolution, aberration, and noise are analyzed. e *2(XXJ Society of Photo-Optical Instrumentation Engineers.* [50091-3286(00)00411-6J

Subject terms: optical information processing; image rotation; parallel processing; pattern recognition; acousto-optic beam deflector.

Paper 990289 received July 26. 1999; revised manuscript received Feb. 21, 2000; accepted for publication June 1, 2000.

1 Introduction

Image rotation is important for various image manipulation applications such as rotation-invariant pattern Recognition, computer graphics, virtual reality, and 3-D visualization.

Currently image rotation is normally achieved by computer algorithms and is time-consuming. Several optical methods have been proposed for high-speed optical image rotation.2-7 We also proposed a nonmechanical method using an acousto-optic dove prism (AODP) that consists of two crossed acousto-optic beam deflectors and a polygon mirror. In our previous work, we used two mirrors oriented perpendicular to each other just to prove the concept of the idea for two different rotation angles.8

In this paper, we describe an experimental demonstration of nonmechanical optical image rotation to 20 different angles in a programmable manner, for the first time to our knowledge. The improved optical system consists of a custom-made cylindrical comer cube polygon mirror (C3-PM) with 20 facets within a half cylinder and a 2-D acousto-optic beam deflector.

2 Basic Concept of the AODP

The concept of nonmechanical image rotation using an AODP was published previously8 and its overall schematic diagram is shown in Fig. 1(a). Briefly described, light from a laser source is expanded and illuminates an input image. Light passing through the input is diffracted by the first 2-D acousto-optic beam deflector (AOBD) that consists of a crossed acousto-optic Bragg cells oriented along the *x* and y directions. The diffracted light is then focused by lens L 1 on the surface of one of the facets of an internal polygon mirror. The light reflected from the mirror facet is then diffracted by the second 2-D AOBD, which is identical with the first one with the same acoustic frequencies. The rotated version of the original image is formed at the focal plane of lens L2.

The acoustic frequencies applied to the first and second 2-D AOBDs are the same but along opposite directions and the system is symmetric with respect to the center of the polygon mirror. Therefore, all the dispersion effects caused by the first 2-D AOBD are compensated by the second 2-D AOBD and the output light from the second 2-D AOBD is fixed along the same direction, regardless of rotation angles. This enables pure image rotation without a translational displacement.

To save optical components and to make an AODP compact, the system can be folded simply by adding a mirror just after the polygon mirror and a beamsplitter between an input and the first 2-D AOBD, as shown in Fig. l(b).

3 Components

The AODP mainly consists of two components: 2-D AOBDs and a polygon mirror. 10 the following, a detailed description of the components is provided.

3.1 *2-D AGBD*

The requirements of a 2-D AOBD are illustrated in Fig. 2. First, it should be able to diffract incident beam over a wide range of sweep angles. This requires a wide-frequency bandwidth and slow acoustic velocity. As is explained later, bandwidth is directly related with the available number of different rotation angles and resolution of an image. In general, the beam sweep angle is given by $\Delta\theta=\lambda\,\Delta f/v$, where λ, Δf, and v represent the wavelength of light, frequency bandwidth, and phase velocity of sound, respectively. To increase the attainable sweep angle, one should find an acousto-optic material with a large-frequency bandwidth and a slow acoustic velocity. Second, the 2-D AOBD for this application should have a wide input angular bandwidth so as not to cause spurious striation in the diffracted light beam. Note that incoming beam onto the AOBDs in this case is not collimated but instead is focused with a

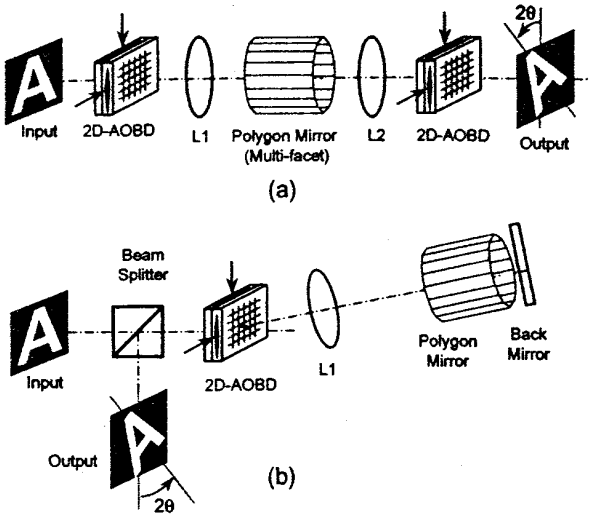

Fig. 1 (a) AODP and (b) its folded version using a c3.PM.

wide angular bandwidth. Third, the AOBDs should have high diffraction efficiency to enable high light throughput. Since the AODP requires four AOBDs in series, even a small difference in diffraction efficiency of a single device can result in a significant difference for the whole system. Fourth, the device should have a large optical aperture size not to block light from 2-D images. Fifth, the distance between the two AOBDs must be short enough so that the beam diffracted by the first AOBD is still within the optical aperture of the second AOBD. Finally, all the AOBD surfaces must be antireflection coated. This is important especially in the folding geometry because the noise due to reflection from the AOBD surfaces propagates along the same direction as signal.

3.2 *C3-PM*

The polygon mirror and the back mirror in the folded scheme can be attached together to make a compact C^3-PM. The requirements of a C^3-PM are illustrated in Fig. 3. First, to keep the center of rotated images unchanged, all the *mirror* facets of a polygon must be oriented precisely parallel to the optical axis and the back mirror must be normal to the facets to form an array of corner cubes that consists of a back mirror and each of the polygon mirrors. The angle between the two mirrors forming a corner cube must be precisely 90 deg to keep the displacement of an

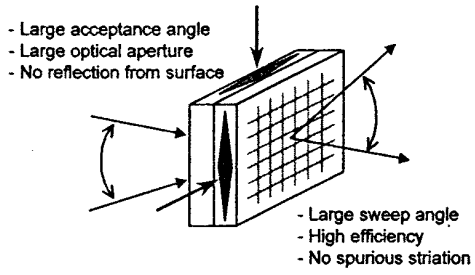

Fig. 2 Requirements of a 2-D AOBD

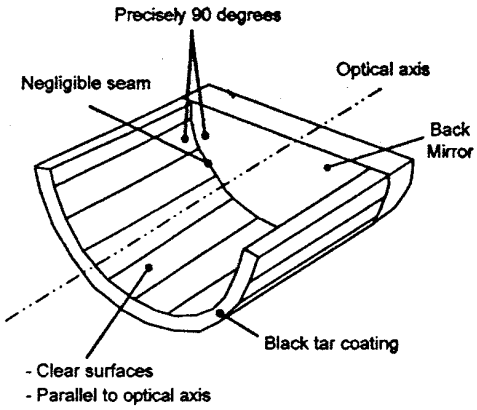

Fig. 3 Requirements of a C3.PM.

output image negligible. The angular tolerance of a polygon mirror is given by $\Delta\theta \leq \Delta x/f_L$ where Δx is tolerable displacement of the center point of an image at the output plane, and f_L is the focal length of lens L1. The tolerable displacement depends on applications but typical values of $\Delta x = 10\mu m$ (1 pixel size) *and* f_L = 100cm will end up with angular tolerance of 10-5 rad or 2 arcsec, which can be met with commercially available retroreflectors that typically have 1 arcsec of deviation.

4 Experiments

4.1 *Experimental Setup*

Figure 4 shows a schematic diagram [Fig. 4(a)] and a photo [Fig. 4(b)] of our experimental setup. Light from a 10-mW HeNe laser is expanded and illuminates an input mask (resolution chart). The beam is then diffracted by a 2-D AOBD and is focused by a lens on the surface of the c3-PM. The reflected light retraces back to the original light path and is detected by a CCD after a beamsplitter.

The positions of the 2-D AOBD and lens Ll can be interchanged without significantly affecting performances. In both cases, however, it is convenient (not mandatory) to position the input mask exactly at the front focal plane of the lens using the autocollimation technique so that the system can keep 1: 1 symmetry with respect to the C3-PM.

A pair of *x-y* frequency synthesizers interfaced with a PC generates rf frequencies to control beam direction. The C^3-PM is carefully mounted at the focal plane of lens L1 on a mount with *xyz* translation and rotation/tilt controls. The

rotation and tilt angles of the C^3-PM are adjusted so that

light diffracted by the center frequencies hits the center of the back mirror and retraces its original path. Acoustic frequencies are carefully chosen so that the beam hits the desired corner cube and retraces to the original light path again. Once the frequencies are found, a look-up table is set up to automatically select the set of *x-y* frequencies for the desired rotation angle.

4.2 *2-D AOBDs*

The 2-D AOBD used in this experiment consists of a pair of identical l-D Bragg cells made of TeO_2 shear wave ma

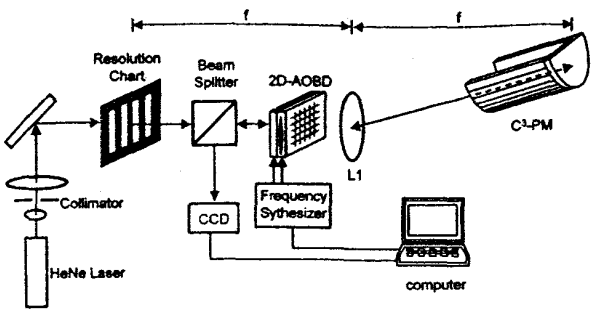

(a)

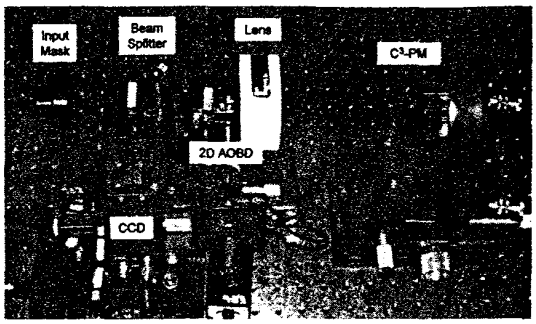

(b)

Fig. 4 Experimental setup of an AODP: schematic diagram (a) and photo (b).

terial (NEOS, N45090-2D, 8 X 8 mm).* The center frequency and FWHM bandwidth of the AOBDs are 100 and 60 to 80 MHz, respectively. To obtain broad input angular bandwidth, each AOBD has a narrow diamond-shaped transducer to reduce the width of the acoustic beam along the light propagation direction. This relaxes the volume effect *(Q* factor) and accordingly striation effect as well. Nonetheless, maximum diffraction efficiency of an AOBD is approximately 40 and 16% for I-D and 2-D operations, respectively, at the HeNe wavelength at 1 W rf power. The frequency bandwidth of an AOBD highly depends on the tilt angle of the device and is shown in Fig. 5 for five different angles around the Bragg angle. With a careful adjustment, we could obtain a bandwidth of almost 80 MHz at FWHM.

We also tried a compact 2-D AOBD with two orthogonal transducers on the same crystal. The device worked well except for the striation effect and low efficiency. Typical efficiencies were 14 and 0.2% for single and two directions, respectively, at 1 W rf power. The low efficiency for two dimensions is expected because individual adjustment of Bragg angles is not available with this device. Also, the crystal axis of the AOBD must be oriented between the two directions, compromising light efficiency.

*No approval or endorsement of any commercial product by the National Institute of Standards and Technology is intended or implied. Certain commercial equipment, instruments, or materials are identified in this paper to facilitate understanding. Such identification does not imply recommendation or endorsement by the National InstitUte of Standards and Technology. nor does it imply that the materials or equipment identified are necessarily the best available for the purpose.

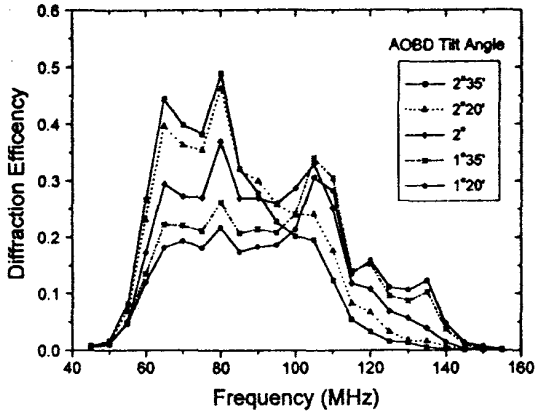

Fig. 5 Diffraction efficiency (and hence bandwidth) of an AOBD for various crystal angles.

4.3 *cJ-PM*

Figures 6(a) and 6(b), respectively, show a schematic diagram and a close-up photo of the custom-made polygon mirror with a backmirror attached to it (manufacturer: Coastal Optics). It has 20 facets in a half cylinder, fonning an angle between the adjacent mirror facets of around 171 deg. Special care was taken to meet the requirements described previously. Especially the backmirror is kept precisely normal to each of the mirror facets to ensure retroreflection. Also, the seams between mirrors were made as small and invisible as possible.

5 Experimental Data

Figure 7 shows 20 different rotated versions of an input image (a resolution chart) experimentally obtained from the AODP system. The rotation angle between adjacent images is 18 deg-twice the difference in angles between the normals of adjacent mirrors. This result clearly demonstrates the concept of the nonmechanical image rotation into a reasonably large number of angles.

One can also see that the resolution of the output images is degraded compared with the original image. Some of the sources of image degradation including resolution and other background noises are described later in Sec. 6.

6 Discussion

6.1 *Maximum Number of Rotation Angles*

The maximum number of rotation angles using the proposed AODP is determined by the spectrum size of an input image relative to the diameter of the circle swept by the 2-D AOBD at the polygon mirror plane. The size of a spectrum is given by $w = \lambda(f_L/S_{min})'$ where S_{min}, f_L, and λ are the minimum feature size (a half of a period) of an input image, the focal length of lens L1, and the wavelength of light, respectively. The sweep distance by an AOBD is given by $\Delta x = f_L\lambda(\Delta f/v)$, where AI is the acoustic frequency bandwidth. Therefore, the number of rotation angles, N is given by

'See preceding footnote.

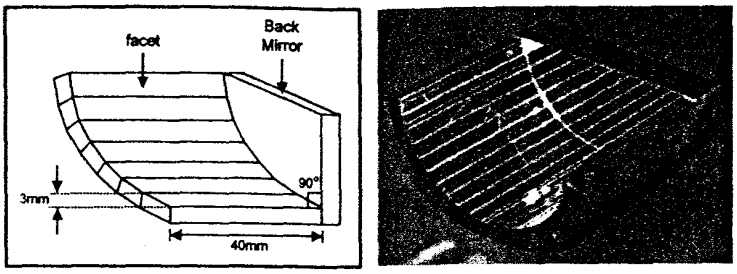

(a) (b)

Fig. 6 C3-PM: (a) schematic and (b) photo.

$$N=\frac{\pi\Delta x}{w}=\frac{\pi f_L\lambda(\Delta f/v)}{\lambda(f_L/s_{\min})}=\frac{\pi\Delta f s_{\min}}{v}.$$

Note here that N is independent of the wavelength or the focal length of the lens. Also, note that the full circle can be used without redundancy by shifting the angles of mirror facets in the second circle by half of the angle between neighboring mirrors to avoid duplication in rotational angles. Plugging in the typical values of Δf= 50 MHz, S_{min}=*0.1* mm, and *v=617m/s, N* becomes 25.

This number can be increased either by using a suitable acousto-optic material with larger $\Delta f/v$ ratio or by using higher order diffraction. For instance, by using an acousto-optic beam deflector made of shear-mode LiNbO3 with Δf= 1 GHz and v=3500mls, the $\Delta f/v$ ratio can be increased by four times compared with that in the preceding example using a shear-mode TeO2 AOBD. This can result in approximately 100 different rotation angles. The $\Delta f/v$ ratio is related with time-bandwidth product (TBP), which is given by $D\Delta f/v$, where D is the aperture size of an AOBD. Also, the phased-array transducer geometry can be used to increase the bandwidth even further. In addition, if the third-order diffraction is used, for instance, instead of the first order, the number N increases by another three times. However, such higher order diffractions have significantly less diffraction efficiencies compared with the first

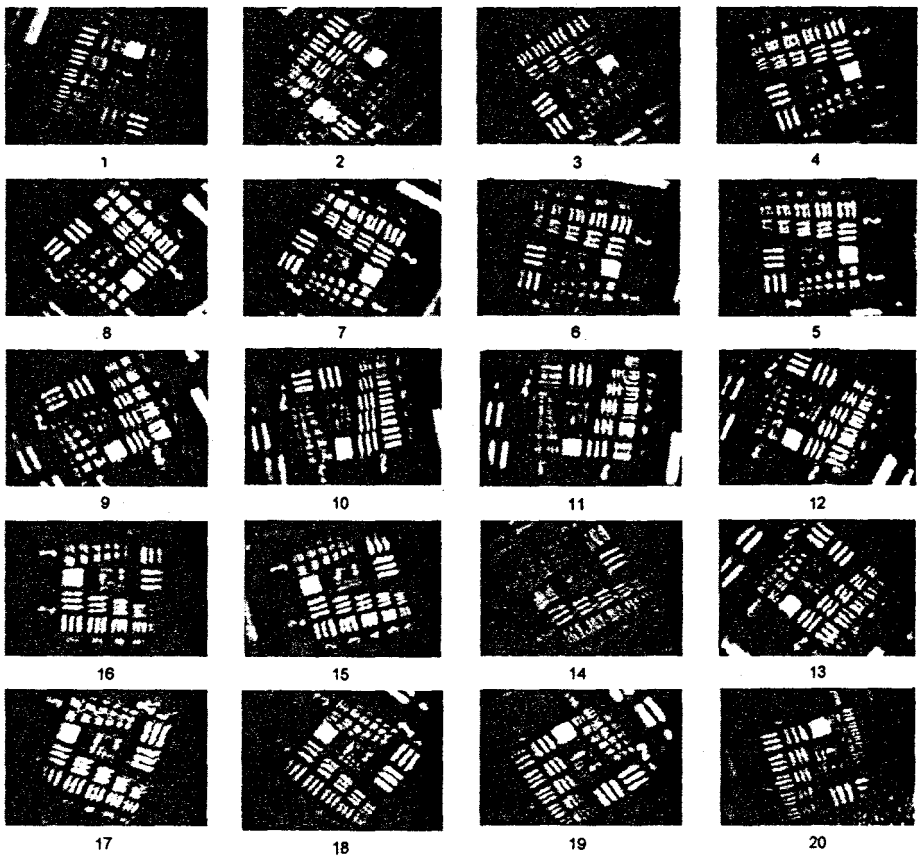

Fig. 7 Experimental demonstration of nonmechanical image rotation to 20 different angles.

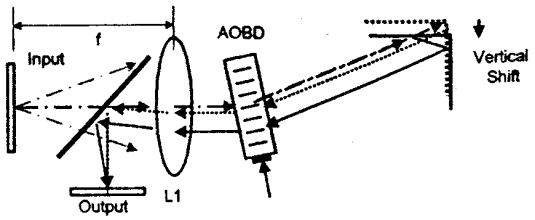

Fig. 8 Crosstalk due to higher order diffraction.

order diffraction. Also, a spatial filter must be used to block unwanted diffraction orders.

6.2 *Image Resolution*

Resolution of an image is dependent on directions along the length and tangential directions of a C3-PM. This is because the imaging system has two different aperture sizes along the two directions. The effective aperture size is determined by the dimension of the projected area of each mirror facet on a plane normal to the light propagation. The two different aperture sizes determine two different resolutions of an image along the two directions. To match resolution along both directions, we designed a C3-PM with an appropriate ratio between the length and width of a mirror facet for a given diffraction sweep angle.

6.3 *Light Efficiency*

The main source of light loss in an AODP is the AOBDs since light should pass through four AOBDs in series. Diffraction efficiency of an AOBD is typically about 50% (3 dB loss) and so passing through *four* AOBDs results in a 12-dB loss *(6.25%* efficiency). Furthermore, if the device is operated beyond the frequency bandwidth to increase the sweep angle, efficiency will drop accordingly.

6.4 *Effects of Beam Position on ad-PM on Image Displacement*

One might wonder whether the center of the input beam should be exactly at the comer of a comer cube to avoid displacement of the center of output images in the folded scheme. This is not true and is explained in Fig. 8. Light from a point source in the input plane is collimated by lens L1, which is separated from the input mask by a focal length. The collimated light is then diffracted by the AOBD and is reflected by a comer cube and is bounced back. In the figure, the dotted line represents light reflected near the comer and the solid line represents light reflected from a point away from the comer. While the two beams (dotted and solid lines) are displaced from each other, the directions of the reflected light are the same, and so both beams are focused at the same point at the output plane. Therefore, it is not necessary for the beam to be reflected from a corner. This is important because it is normally difficult to make a perfect seam without a noticeable irregular scatterer. The only thing to keep in mind is to keep the displaced reflected beam within the optical aperture of the AOBD.

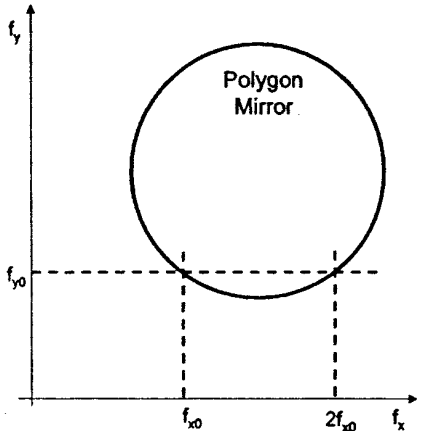

Fig. 9 Effect of beam position on the surface of the c3-PM on the displacement of output images.

6.5 *Crosstalk Due to Higher Order Diffraction*

The crosstalk noise due to higher order diffraction is illustrated in Fig. 9. For a certain frequency pair (f_{x0}, f_{y0}), the second-order diffraction $(2f_{x0}, f_{y0})$ also strikes the surface of a polygon mirror. Sometimes 'even higher order diffraction can be on the surface of the polygon mirror. However, these higher orders are normally weak, and so their effects are negligible. Furthermore, these higher order effects can be completely removed if $\Delta f < (2/3)f_c$, where Δf and f_c represent frequency bandwidth and center frequency, respectively.

6.6 *Background Noise Due to the Reflection from the Surface of Optical Components*

When the folding scheme shown in Fig. l(b) is used, a noise beam due to unwanted reflection from the surface of optical components propagates along the same direction as the output signal beam and degrades images. Such noise becomes more noticeable when the diffraction efficiency of an AOBD is low and thus the signal beam is weak. Therefore, all the optical components including a beamsplitter, AOBDs, and lenses must be antireflection coated. Some of the reflection noise can be removed by intentionally tilting optical components so that the reflected beam does not overlap the signal.

6.7 *Effects of Separation between Two AOBDs*

As discussed, it is highly desirable for the crossed AOBDs to be situated as closely as possible to avoid beam walkoff. This will ensure the beam diffracted by the first AOBD to reside well within the optical aperture of the second AOBD. The separation between the two AOBDs, d should satisfy the relationship $d<<(av/\lambda\Delta f)$, where a is the optical aperture size of the first AOBD. The equation is obtained from the simple relationship $d \sin(\Delta\theta)<<a$. As an example, for a= 1 cm, $\Delta\theta$ =80MHz, v=617m/s, and λ = 0.633 ,μm, the separation has to be much less than (approximately 10% of) 12 cm.

7 Conclusion

We demonstrated an experimental nonmechanical image rotation to 20 different angles in a programmable manner, for the first time to our knowledge. Also, various theoretical limits of the system including the maximum number of rotation angles, resolution, light efficiency, and crosstalk noise are discussed. Most of these limitations are not fundamental and future high-speed large-angle beam deflectors would enable full utilization of our AODP concept.

Acknowledgment

This work was supported by the u.s. Office of Naval Research (ONR) under Contract No. NCOO14-97-F-OO21.

References

I. M. Unser. P. Thevenaz. and L. Yaroslavsky, "Convolution-based interpolation for fast high-quality rotation of images," *IEEE Trans. Image Process.* 4(10), 1371-1381 (1995).

2. R. B. Johnson. "Image mation device for an infrared sc:anning~ tern or the like:' *AppL Opt.* 13,2962 (1974); "Image rotation deviCe' for an infrared scanning system or the like," U.S. Patent NO: 3,813,552 (May 28, 1974). ,;,
3. W. G. McKinley, "Non-polarizing image rotation apparatus ~ method," *Appl. Opt.* 33, 6570 (1994); "Non-polarizing image rotation apparatus and tnethod," U.S. Patent No. 5,296,972 (March 22, 1994).
4. R. H. Ginsberg, "Image rotation." *AppL Opt.* 33, 8105 (1994).
5. B. Braunecker, O. Bryngdahl, and B. Schnell, "Optical system foc image rotation and magnification." *J. Opt. Soc. Am.* 70, 137-141 (1980).
6. A. W. Lohmann, "Image rotation. Wigner rotation, and the fractional Fourier transform." *J. Opt. Soc. Am. A* 10, 2181-2186 (1993).
7. A. Chiou and P. Yeh, "Scaling and rotation of optical images **using.** ring cavity," *Appl. Opt.* 29, 1584-1586 (1990).
8. E. G. Paek, J. Y. Choe, T. K. Ob, J. H. Hong, and T. Y. Chang.. "Non-mechanical image rotation." *Opt. Len.* 22, 1195-1197 (1997).

Biographies of the authors not available.